RSC Advances

PAPER

View Article Online
View Journal | View Issue



Cite this: *RSC Adv.*, 2021, **11**, 17760

# Nanoflakes of chloride zinc–iron–aluminum-based layered double hydroxides obtained from industrial waste: a green approach to mass-scale production

Larissa Bello Neves de Farias,[a] Gregorio Guadalupe Carbajal-Arízaga,[b] Luis Guilherme Giannina Sante,[a] Luciane Effting,[c] Juliana Aparecida Correa da Silva Fernandes[a] and Alesandro Bail *[a]

A greener technology aiming at a smarter industrial waste treatment is proposed to produce chloride iron–zinc–aluminum layered double hydroxides (LDHs). Waste Pickling Acid (WPA) and sodium aluminate ($NaAlO_2$) from secondary sources were meticulously mixed under mild experimental conditions using a sodium hydroxide solution as a pH-regulator. A set of characterization techniques (XRD, SEM, TGA, FTIR, AAS and adsorption–desorption of $N_2$) indicated the formation of highly-dispersed nanoflake crystallites with textural characteristics and thermal stability similar to syntheses with high-quality chemicals. An interesting discussion on chemical composition and $M^{2+}/M^{3+}$ molar ratio is presented. Although the co-precipitation synthesis was conducted without control of environmental $CO_2$, complete intercalation of the chloride anion was achieved, making these particles more favorable for further anion exchange applications. The experimental variables temperature of reaction and WPA/$NaAlO_2$ volume ratio showed the strongest influence on the LDHs crystallinity and porosity. LDHs architected with iron and zinc have the potential to be applied in systems for removing sulfur gases for cleaner energy production, *e.g.* in the refining process of biogas to produce biomethane.

Received 13th February 2021
Accepted 9th May 2021

DOI: 10.1039/d1ra01201k

rsc.li/rsc-advances



## 1 Introduction

The 2030 Agenda for Sustainable Development of the United Nations is related to 12 Principles of Green Chemistry, in particular with regard to the establishment of more-sustainable and waste-free processes.[1,2]

It may seem that, from the point of view of green chemistry, converting industrial waste into an advanced material sounds like the work of a successful alchemist's turning a base metal into gold.[3] Notwithstanding, technologies for the recovery of waste are a smart strategy to mitigate the effects of pollution and improve the economy for workers and entrepreneurs.[4–6]

Waste Pickling Acid (WPA) is an industrial waste generated during the removal of iron oxide layers from the crude steel surface.[7] The global metallurgical industry depends on this process to manufacture steel for metal products, building and infrastructure, automotive parts, mechanical equipment, transport sector, among many others.[8] According to the World Steel Association (WSA), the global production of crude steel grew 10 times from 1950 to 2019, reaching 1.8 billion tons during the year.[9] The amount of WPA is expected to grow in parallel with the steel production, which in turn is closely linked to the economic growth of countries.[10]

The European Union produces $300 \times 10^3$ $m^3$ of WPA per year and stores $150 \times 10^3$ tons per year.[11] Despite the numerous alternative methods reported in the literature,[12–15] the simple precipitation with lime has been the most common treatment at industrial scale.[16] However, this precipitation shows significant technical drawbacks, such as the low capacity to recover the metals and the disposal of iron hydroxide/oxide sludge in landfills or exposed places to several weather conditions, which leads to the contamination of the soil and water.[17] It was estimated that *ca.* of 10% of all WPA treated volume results in sludge containing a mixture of iron hydroxide and iron oxide.[18] Besides, depending on the origin, the sludge may contain other metals such as zinc, nickel, chromium and lead.[19] Metals like zinc, iron and aluminum are abundantly found in industrial waste and could be reused from WPA to engineer advanced materials with multiple applications such as layered double hydroxides (LDHs), LDHs are materials formed by the stacking of layered units resulting from the combination of different metallic ions, and exchangeable interlayer anions that bind the stacking.[20,21] Generally, an LDH layer is formed by divalent and trivalent metal ions ($M^{2+}$ and $M^{3+}$) coordinated to hydroxyl

[a]*Grupo de Química de Materiais e Tecnologias Sustentáveis (GQMATS), Universidade Tecnológica Federal do Paraná (UTFPR), CEP: 86036-370, Londrina, Paraná, Brazil. E-mail: alebail@utfpr.edu.br*

[b]*Departamento de Química, Universidad de Guadalajara (UDG), C.P. 44430, Guadalajara, Jalisco, Mexico*

[c]*Departamento de Química, Universidade Estadual de Londrina (UEL), CEP: 86050-482, Londrina, Paraná, Brazil*

groups with a typical $M^{2+}:M^{3+}$ molar ratio of 2 : 1, 3 : 1 or 4 : 1.[22] The presence of trivalent cations produces a charge residue that is neutralized by interlayer anions. Such anions can be exchanged in liquid media or in solid state reactions.

LDHs present a high anion exchange capacity (AEC), making it possible to replace small anions by even large organic anions, promoting the expansion of the interlayer distance.[23,24] The modification with organic species allow for designing advanced pollutant adsorbents.[25]

The high AEC is limited by interlayer carbonate ions ($CO_3^{2-}$), which present a higher affinity for the positive charge residue in the layers due to the high charge density.[26] The relative affinity sequence of interlayer anions is shown below:[21,27]

$$CO_3^{2-} > SO_4^{2-} > OH^- > F^- > Cl^- > Br^- > NO_3^- > I^-$$

In fact, to overcome the thermodynamically favored intercalation of the carbonate ion, the synthesis of the LDHs has to be carried out under $CO_2$-free atmosphere, which involves relatively careful experimental procedures.[28] In this sense, the development of a green technology using industrial waste as the metal cations source to produce LDH structures with chloride ions is an attractive option to obtain high-value LDH materials.

Unlike the most common LDHs (those prepared from magnesium, aluminum and zinc salts), the synthesis of iron-based LDHs is still underexplored. A particular case concerning the combination of $Fe^{2+}$ and $Fe^{3+}$ – named green rust, suggests that the low stability of the ferrous ion in an oxygen-rich environment could compromise the structure.[29] In fact, the green rust synthesis usually consider the use of oxidizing or reducing agents to modulate the composition of ferrous ($Fe^{2+}$) and ferric ($Fe^{3+}$) ions under delicate conditions.[30] Nevertheless, some successful syntheses of iron-based LDHs and their potential have been reported. In one study, the $Mg_4FeAl$–Cl and $Zn_4FeAl$–Cl, in which all the iron corresponded to $Fe^{3+}$ ions, were carefully prepared under nitrogen atmosphere and dried under reduced pressure to minimize the carbonate content. In this procedure, the presence of $Al^{3+}$ and $Zn^{2+}$ could avoid impurities of iron oxo-hydroxo phases and enhance the LDH crystallinity.[31]

Another study has reported the use of an acidic residual solution as an iron source plus a high purity source of magnesium in the synthesis of LDHs. The $Mg_4Fe$–$CO_3$ LDH was prepared by co-precipitation at low oversaturation with 1.0 mol $L^{-1}$ $Na_2CO_3$ and 2.0 mol $L^{-1}$ NaOH solutions. The 20 hour reaction produced a single crystalline phase product with porous structure.[32]

LDHs are known for their outstanding capacity to intercalate carbonate ions and their potential to be used as $CO_2$ scavengers in gaseous mixtures.[33,34] Although this is the most common feature of LDHs, the iron–zinc-based LDHs present a high potential to be applied as adsorbents for the removal of $H_2S$ and biogas purification. Recently, Lee *et al.* synthesized Co–Fe-based LDH and its high removal capacity of $H_2S$ under high humid gas stream achieving up to 247 mg $H_2S$ $g^{-1}$ Co–Fe–LDH. The authors proposed an adsorption mechanism in which the $H_2S$ molecules could react with the $CO_3^{2-}$ ions to form $HS^-$ and $HCO_3^-$. Despite the surprising results, the reported chemisorption between sulfur and metal could be better understood by including the participation of other intercalated anions instead of $CO_3^{2-}$.[35]

In this study, we present a green and facile technology based on the conventional co-precipitation method with view to producing zinc–iron–aluminum based-LDHs intercalated by chloride anions using WPA and $NaAlO_2$ from secondary sources. We expect these materials will be useful in biogas purification processes since the iron and zinc could function as potential adsorption sites for sulfur-containing molecules.

## 2 Experimental

### 2.1. Chemicals

Sodium hydroxide, purity >97 wt% was purchased from Neon (Brazil). The waste pickling acid (WPA) and sodium aluminate solution ($NaAlO_2$) >95 wt% were supplied by a local company in polypropylene flasks. The WPA was previously characterized[36] and presented the following metal content: Fe 10.8 wt% and Zn 7.42 wt%; Cr, Pb and Ni 26.6, 73.4 and 14.0 mg $L^{-1}$, respectively. The process details on $NaAlO_2$ production from aluminum scraps are protected by the local company, however, the $NaAlO_2$ used in this work presented aluminum content of 13.2 wt%.

### 2.2. LDH synthesis

The LDH was prepared by the co-precipitation method employing the iron-and-zinc-containing industrial waste under variable pH. The synthesis was performed in a 1000 mL glass container with magnetic stirring; temperature and WPA/$NaAlO_2$ molar ratio were controlled (Table 1).

A typical description of the synthesis could be as follows: 50.0 mL of WPA was filtered under low pressure in order to remove the steel chips, plastic pieces and other large impurities. The adequate volume of $NaAlO_2$ was slowly added under magnetic stirring (~500 rpm) and constant temperature. A greenish brown sludge was observed and when the pH reached the range 10–11 by the dropwise addition of an NaOH 1.0 mol $L^{-1}$ solution, a dense precipitate was formed. After the

Table 1 Experimental conditions for the LDHs syntheses[a]

| ID | $NaAlO_2$ (mL) | $\frac{M^{2+}}{M^{3+}}$ | Time (h) | Temperature (°C) |
|---|---|---|---|---|
| LDH-1 | 35.0 | 1.8 | 4.0 | 60 |
| LDH-2 | 35.0 | 1.8 | 4.0 | RT |
| LDH-3 | 35.0 | 1.8 | 0.5 | 60 |
| LDH-4 | 35.0 | 1.8 | 0.5 | RT |
| LDH-5 | 25.0 | 2.6 | 4.0 | 60 |
| LDH-6 | 25.0 | 2.6 | 4.0 | RT |
| LDH-7 | 25.0 | 2.6 | 0.5 | 60 |
| LDH-8 | 25.0 | 2.6 | 0.5 | RT |

[a] Volume of WPA = 50.0 mL; RT = room temperature (~25 °C); magnetic stirring ~500 rpm; $M^{2+}/M^{3+}$ = theoretical molar ratio, where $M^{2+} = n_{Fe} + n_{Zn}$ and $M^{3+} = n_{Al}$.

required reaction time, the precipitate was filtered under low pressure and washed by distilled water until pH 7–8. The supernatant of the reaction mixture was reserved for further evaluation. The greenish brown cake was dried at 70 °C overnight, leading to the formation of a light brown material. The dry cake was grounded in a mortar and sieved in order to control the particle size in the range 75–150 μm. The powder was stored in flasks and labeled from LDH-1 to LDH-8, according to the experimental condition that led to its formation.

### 2.3. LDH characterization

Powder X-ray diffraction analysis (PXRD) was conducted in a Bruker D2 Phaser diffractometer operating at 30 kV and 40 mA with copper radiation (Cu-K$\alpha$ = 0.15418 nm) in the range 5–50° with dwell time of 2° $min^{-1}$.

Scanning Electron Microscopy (SEM) was recorded in a FE-SEM, TESCAN model VEGA 3.

Transmission Fourier Transform Infrared (FTIR) spectra were registered on a Perkin Elmer FTIR spectrometer model Frontier in the range 400–4000 $cm^{-1}$, using KBr pellets. KBr was ground with a small amount of the solid to be analyzed, and the spectra were collected with a resolution of 4 $cm^{-1}$ and accumulation of 32 scans.

Adsorption/desorption of $N_2$ analysis was performed in order to measure the specific surface area, the average pore diameter and the pore volume of the LDHs. For this purpose, the BET[37] and the BJH[38] methods were applied to the corresponding nitrogen desorption isotherms, which were collected on an ASAP 2020 N Automatic Physisorption Analyzer from Micrometrics at 77 K. The samples were previously degassed by treatment at 110 °C until the system pressure had achieved 10 $\mu m_{Hg}$. The nitrogen adsorption data were obtained by using approximately 0.1 g of the sample.

Thermogravimetric analysis (TGA) was performed on a Perkin Elmer simultaneous 195 thermal analyzer model STA 6000, where approximately 10 mg of the sample was placed in an open platinum crucible and pre-heated at 100 °C for 5 min. The experiments were carried out in nitrogen atmosphere, at a flow rate of 10 mL $min^{-1}$ and a heating rate of 10 °C $min^{-1}$, in the range 100–650 °C.

Atomic absorption measurements were conducted in a Varian spectrometer model SpectrAA-100, operating in flame mode alternating between the gas mixture air/acetylene and nitrous oxide/acetylene. Aluminum was measured in a Macherey Nagel spectrophotometer – VIS II. All measurements were carried out according to the Standard Methods for the Examination of Water and Wastewater.[39]

The bulk density of the LDHs was estimated by the simple ratio between 5.0000 g of a LDH and the respective volume occupied in a graduated polystyrene flask.

## 3 Results and discussion

### 3.1. Synthesis of the LDHs

Fig. 1 shows the eight-step co-precipitation method used in the conversion of the WPA into LDHs containing iron, zinc and aluminum. The co-precipitation process was started by adding $NaAlO_2$ to the WPA and ended by controlling the pH with NaOH aqueous solution (Fig. 1b–d). The filtration led to the formation of a dark green cake that turned brown after drying in the oven. This color change was an important qualitative parameter for monitoring the chemical speciation of the iron ions, *i.e.* the possible oxidation that could take place to convert tetrachloroferrate(II) ion – $[FeCl_4]^{2-}$, and hexaquachloroiron(III) ion – $[Fe(OH_2)_6]^{2+}$, into hydrate $Fe^{3+}$ ions at oxidizing conditions. As an average measure, each 50.00 mL of WPA yielded 31.8 ± 2.4 g of dry LDH.

### 3.2. Characterization of the LDHs

An important aspect for LDHs is their chemical composition in terms of the molar ratio of metals. LDHs 1 and 8 were chosen to be evaluated in detail because they were synthesized under different reaction times, temperatures and quantities of metals

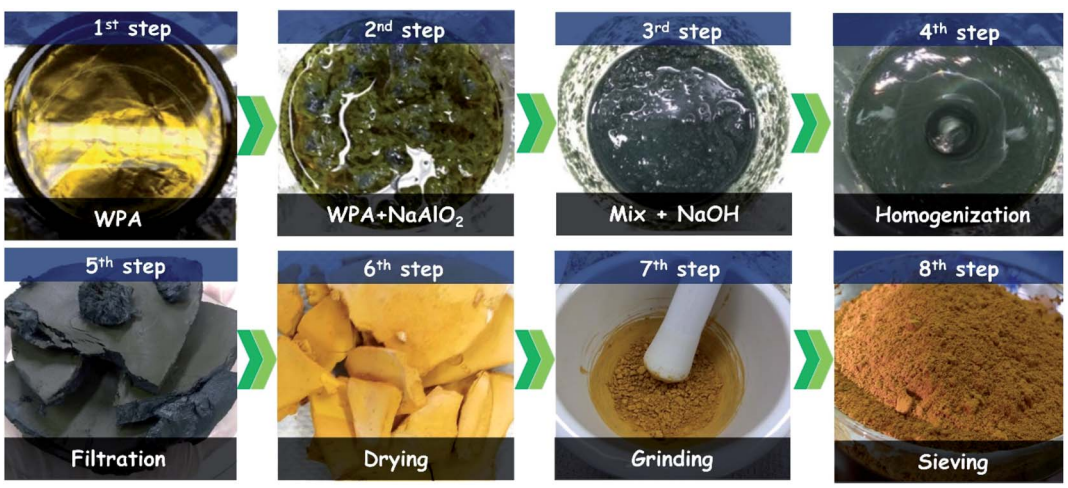


Fig. 1 The eight steps of the LDHs synthesis from industrial waste.

Table 2 AAS results for LDH-1, LDH-8 and the supernatant of LDH-1

| | Metals[a] | | |
|---|---|---|---|
| LDH | Aluminum (%) | Iron (%) | Zinc (%) |
| LDH-1 | 4.73 ± 0.64 | 20.69 ± 0.37 | 15.30 ± 0.18 |
| LDH-8 | 4.34 ± 0.44 | 20.51 ± 0.26 | 16.32 ± 0.03 |
| Supernatant-LDH-1 | 0.029 ± 0.001 | < LD | < LD |

[a] Values represent the percentage of metal per 100 g of LDH (g per 100 g); for supernatant the percentage is expressed in 100 mL (g per 100 mL).

(Table 1). The concentrations of the metals were determined by AAS and the results are presented in Table 2. Since the WPA was generated in the industrial pickling process and the sodium aluminate was produced from low cost sources, six metals (Fe, Zn, Al, Cr, Ni and Pb) were analyzed in order to monitor the level of transport of the contaminants through the synthesis process until the final product.

As can be seen, the limit of detection (LD) for chromium, nickel and lead, 0.20, 0.20 and 0.005 mg $L^{-1}$, respectively, was not reached, indicating a low level of LDH contamination by those metals. Indeed, this result was expected considering that the WPA presented concentration of Cr, Ni and Pb not higher than 75 mg $L^{-1}$ each. The supernatant of the LDH-1, which presented a strongly basic pH, was monitored and the concentration of the metals Cr, Ni and Pb did not reach the limit of detection. In this case, only the aluminum could be measured at relatively low levels, indicating that almost all the aluminum added was consumed in the LDH syntheses. These results suggested that the supernatant could be recycled in the system itself, allowing it to be used as a blend for a fresh NaOH solution.

In terms of chemical composition, several hypotheses were proposed, which are depicted in Fig. 2. This hypothetical approach was necessary due to the probable oxidation process suffered by the $Fe^{2+}$ ions, which was evidenced by the color change from green to light brown observed after the drying process. The first set of bars expresses the hypothesis in which $Fe^{2+}/Fe^{3+} = 1$, that is, half the amount of $Fe^{2+}$ could have been oxidized to $Fe^{3+}$. The other sets represent situations in which the oxidizing process could have occurred less intensely, leading to gradually higher $Fe^{2+}/Fe^{3+}$ molar ratios. In order to form acceptable $M^{2+}/M^{3+}$ molar ratios, the lower and higher limits for $Fe^{2+}/Fe^{3+}$ were arbitrarily defined as 1 and 5, respectively. Therefore, for all the hypotheses considered, the relation $M^{2+}/M^{3+}$ – which is equal to $Zn^{2+} + Fe^{2+})/(Al^{3+} + Fe^{3+}$, was respected. Additionally, any hypotheses in which the iron ions were not a mix of valences were discarded, firstly because of the unlikely $Fe^{2+}$ ion stability, and secondly due to the extremely low $M^{2+}/M^{3+}$ molar ratio (~0.4) that could be generated and would not meet the minimum requirements for forming a stable chemical structure.

Within the considered range, in the case of the LDH-1, the $Fe^{2+}/Fe^{3+} \sim 4$ seems to represent the experimental condition in which the $M^{2+}/M^{3+}$ reached value 2, whereas for the LDH-8, the $Fe^{2+}/Fe^{3+} \sim 3$ was more consistent with the $M^{2+}/M^{3+} = 2$. These results strongly indicated that the availability of aluminum in the reaction has an important role for the LDH structure formation, modulating the oxidation of $Fe^{2+}$ to $Fe^{3+}$. In short, the lower the volume of $NaAlO_2$ used in the reaction, the higher the level of oxidation from $Fe^{2+}$ to $Fe^{3+}$ in order to form a stable chemical structure. Therefore, it was possible to predict that, approximately, 25 and 33% of the $Fe^{2+}$ was oxidized to $Fe^{3+}$ to form LDH-1 and LDH-8, respectively.

Fig. 3 shows the $N_2$ adsorption–desorption results obtained for all synthesized LDHs. According to Gil *et al.* the LDHs presented Type IV isotherms,[40] suggesting that the materials are formed by slit-type mesoporous and a typical hysteresis H3 above $P/P_0 \sim 0.5$. In addition, the heating influenced the pore

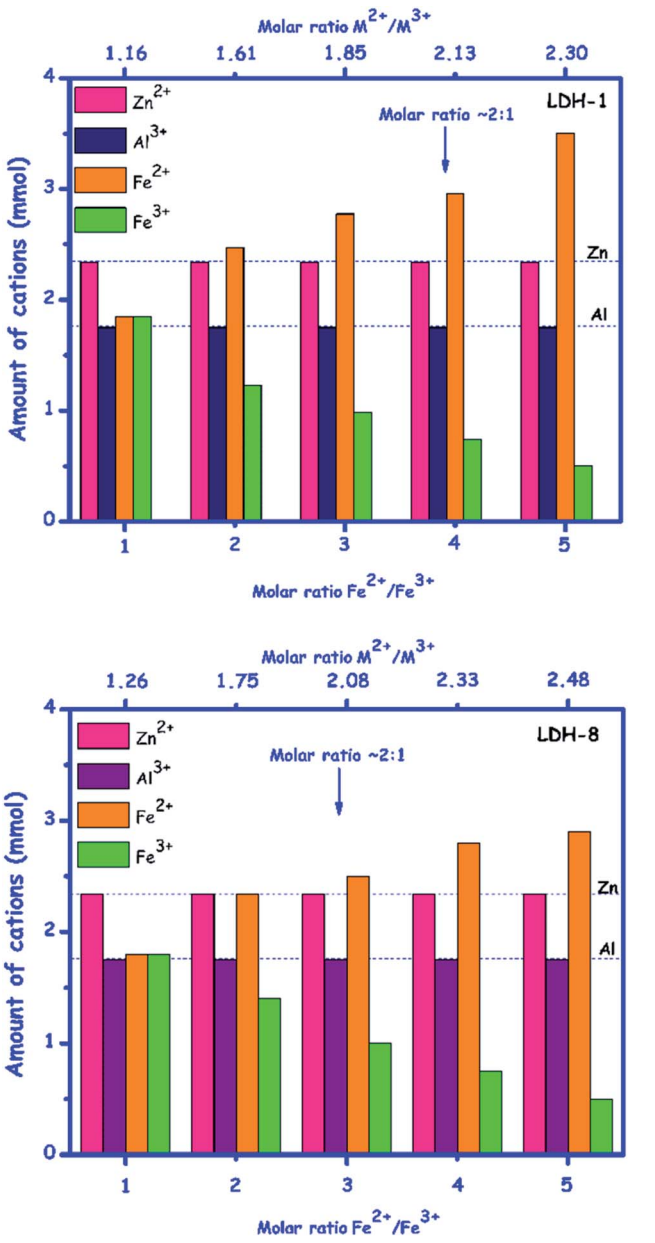


Fig. 2 Hypotheses of the $M^{2+}/M^{3+}$ and $Fe^{2+}/Fe^{3+}$ molar ratios for LDH-1 and LDH-8 samples.

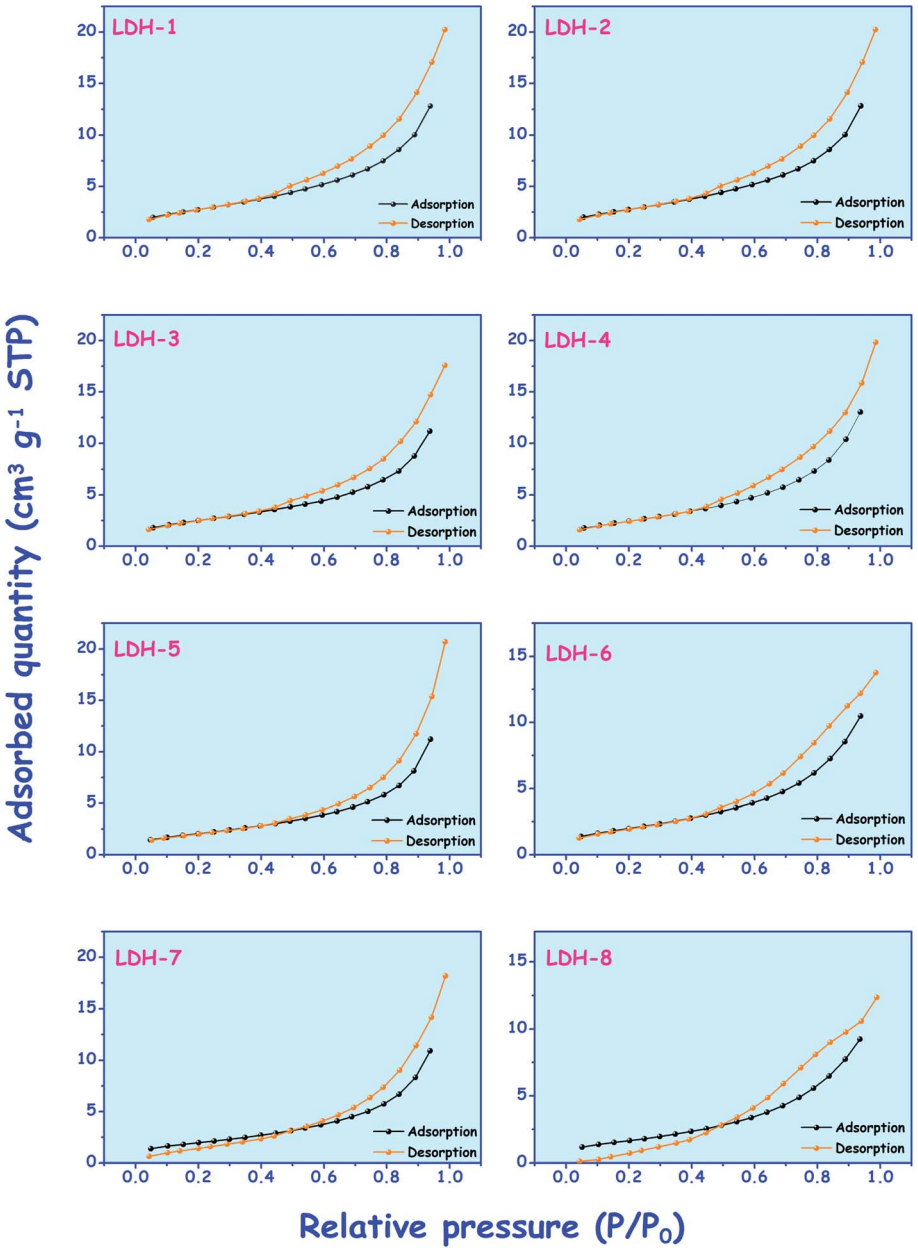


Fig. 3 Isotherms of the LDHs obtained at 77 K.

size distribution (Fig. 4). All LDHs presented pore sizes centered at ~1.8 nm, close to the minimum limit between micro and mesopores. However, LDHs 2, 4, 6 and 8, synthesized under room temperature, showed another distinct region, centered at ~3 nm.

The dependence of both the level of packaging of the LDHs and their textural features to the experimental conditions of synthesis was estimated by the ratio of a mass of LDH and its volume. Table 3 presents the bulk densities and textural results for all prepared LDHs.

Although the eight LDHs have presented a close similarity in their textural properties, LDH-5 and LDH-8 could be highlighted due to the antagonism based on the experimental conditions to which the materials were submitted. LDH-5 showed the highest pore volume (0.28 $cm^3\ g^{-1}$), the highest pore size (8.5 nm) and the lowest bulk density (0.431 $g\ cm^{-3}$). In its turn, LDH-8 showed the lowest pore volume (0.16 $cm^3\ g^{-1}$), one of the lowest pore sizes (6.2 nm) and one of the highest bulk densities (0.777 $g\ cm^{-3}$). In addition, LDH-5 presented a specific area higher than that for LDH-8. Once again, the reaction time extended up to 4 h and the heating to 60 °C seems to have been fundamental in controlling the textural properties of LDHs obtained from WPA.

In terms of the formation and apparent density of the crystallites, it seems that the LDHs syntheses were strongly dependent on all the investigated parameters. The role of the temperature was evident for LDHs 1, 3 and 5. On the other hand, LDH-7 did not follow the same trend, even under heating.

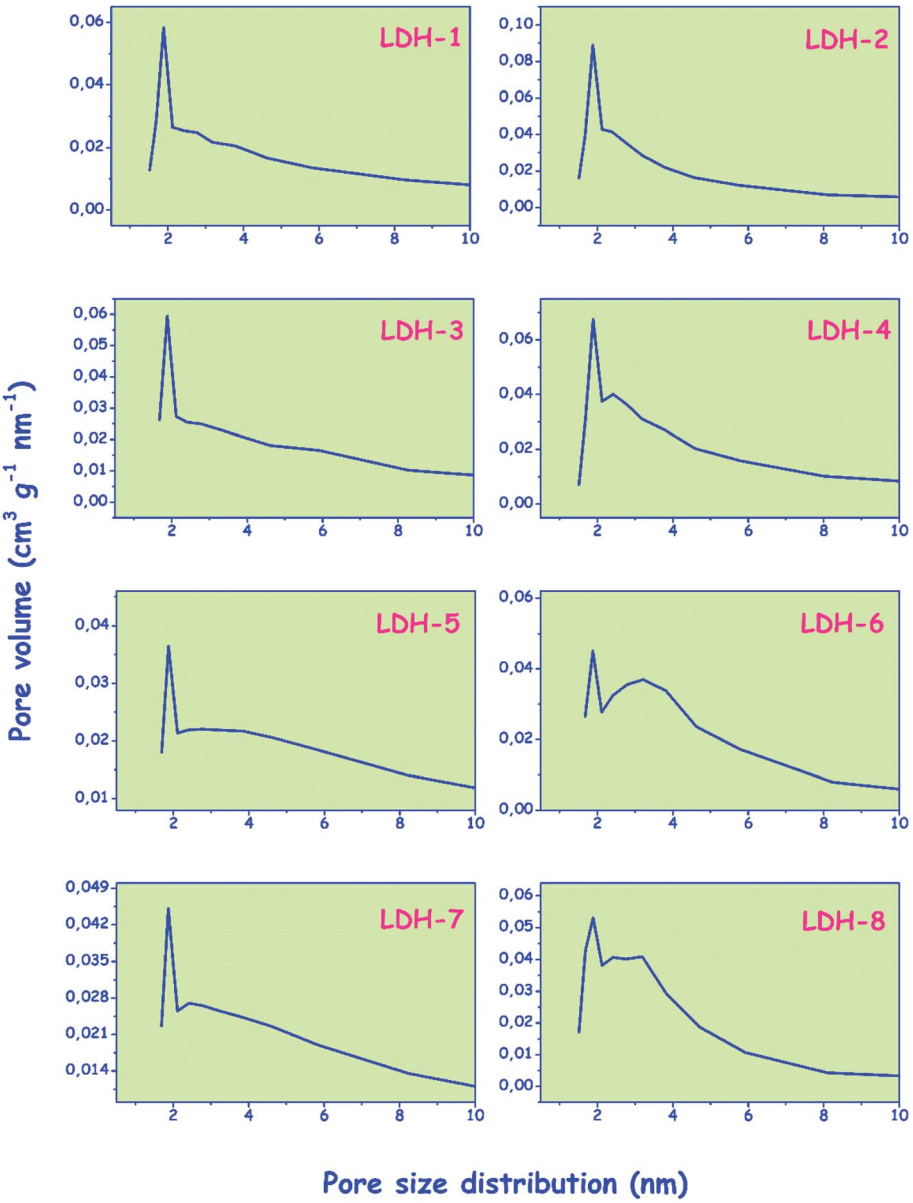


Fig. 4 Pore size distribution of the LDHs from the desorption branch.

Fig. 5 shows the PXRD patterns of the eight synthesized LDHs. The diffraction peaks matched with the LDH profile recorded in the card number 22-0700 of the International Crystallography Diffraction Database (ICDD) and they were identified as the (003), (006) and (012) crystallographic planes of the LDH structure. The discrete peak centered at, approximately, 62° (2$\theta$), corresponding to the metal cations distance, was fundamental to proving the success of LDH preparation with such non-general cations mixture. By means of the Bragg equation, the (110) plane-based distance calculated was ~75 pm, consistent with the ionic radii of the $Zn^{2+}$ and $Fe^{2+}/Fe^{3+}$ in octahedral and low spin coordination, the biggest cations of the metal mixture. The (003) reflection in LDHs prepared under heating (odd labels) were, in general, narrower and with higher intensity, indicating higher crystallinity. As the shape of these peaks is similar, the reaction time tested from the LDH-1 to the LDH-7 did not affect the crystallinity. On the other hand, the peaks in samples prepared at room temperature (even number

Table 3 Bulk densities and textural features

| ID | $\rho_{LDH}$ (g cm$^{-3}$) | Specific area (m$^2$ g$^{-1}$) | Average pore size (nm) | Pore volume (cm$^3$ g$^{-1}$) |
|---|---|---|---|---|
| LDH-1 | 0.463 | 65.5 | 6.1 | 0.20 |
| LDH-2 | 0.655 | 79.8 | 5.3 | 0.21 |
| LDH-3 | 0.532 | 75.5 | 5.9 | 0.22 |
| LDH-4 | 0.591 | 74.4 | 6.7 | 0.25 |
| LDH-5 | 0.431 | 65.8 | 8.5 | 0.28 |
| LDH-6 | 0.963 | 66.3 | 5.8 | 0.19 |
| LDH-7 | 0.478 | 64.8 | 7.8 | 0.25 |
| LDH-8 | 0.777 | 50.7 | 6.2 | 0.16 |

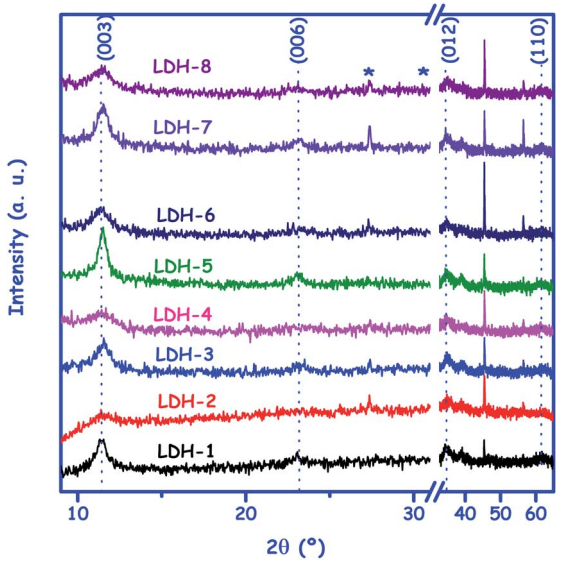


Fig. 5 PXRD patterns for LDHs obtained from WPA. Sodium chloride main peaks have been suppressed.

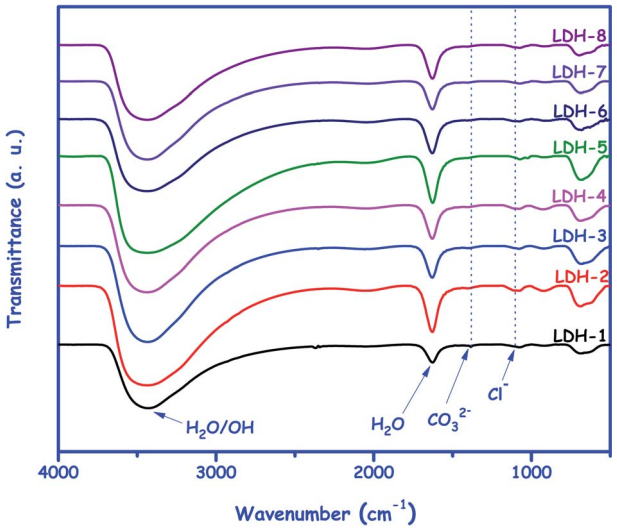


Fig. 6 FTIR spectra for LDHs obtained from WPA confirming the absence of carbonate.

labels) are broader suggesting lower crystal quality or smaller crystal size, which are desirable features for adsorption or anion exchange reactions. Despite the presence of contaminants in WPA and $NaAlO_2$, the PXRD profiles did not reveal formation of secondary phases except that of NaCl. As the intensity of NaCl is high (asterisk in Fig. 5 in matching the ICDD card 77-2064), a break in the axis was needed to give clarity to the LDH profile. NaCl is produced due to the HCl present in the WPA.[41] Even after an exhaustive washing step with abundant water, it was not possible to remove it from the LDH surface, however, the presence of sodium chloride, and then the excess of chlorine ions is responsible for the absence of interlayer carbonate ions, which commonly are observed in chloride-designed LDH. In addition, the interlayer distance calculated from the (003) plane centered at 11.4° by Bragg equation was 7.76 Å, indicating the intercalation by chloride ions.[42] This evidence was confirmed by the infrared data.

Indeed, it has been reported by literature that the concentration of chloride ion in solutions regulates the intercalation process into the interlayer of hydrotalcite-like compounds, even at basic conditions (pH ~10), if the chloride concentration is higher than that for the hydroxide ion, the intercalation of the first will have preference over the second one.[43]

In order to improve the understanding of the intercalation process in the LDHs synthesized from WPA, the FTIR analysis was carried out and its results are shown in Fig. 6. The absence of a strong vibrational band in the range 1350–1390 $cm^{-1}$, typically attributed to a stretching mode of the carbonate ion ($\nu[CO_3]^{2-}$), as well as the weak vibration centered at 1090 $cm^{-1}$, present in all LDHs and attributed to chloride-oxygen stretching (Cl–O), corroborate the intercalation by chloride.[44] In relation to the other bands, the vibrational modes presented by the LDHs revealed a hydrotalcite-like compound of typical structure. The strong and large band in the range of 2900–3700 $cm^{-1}$ was attributed to the stretching of the OH (hydroxyl groups) and $H_2O$ molecules, and the one centered at 1635 $cm^{-1}$ was attributed to the $H_2O$ bending vibration of the interlayer water.[45]

Fig. 7 depicts the TG curves for the eight LDHs in the range 30 to 650 °C. The profiles were as expected for hydrotalcite-like compounds[46] and it was possible to divide them in three regions of mass loss: (1st) from room temperature up to ~200 °C, referring to the water molecules weakly sorbed on the layers surface; (2nd) from ~200 up to ~500 °C, referring to the water molecules intercalated and dihydroxylation, and (3rd) above ~500 °C, referring to the collapse of the structure in order to form a mixture of oxo-hydroxo species. Although the profiles were similar in terms of total mass loss (~27 wt%), the TG curves for LDH-2, LDH-6 and LDH-8 presented a higher rate of mass loss in the first stage, indicating a higher level of hydration in comparison to the other LDHs. This was an interesting result considering that some authors have reported that the LDH capacity to remove $H_2S$ was dependent on the moisture content of the medium.[47]

The SEM images for the LDHs are shown in Fig. 8. At 2000 times of magnification, the LDH-1 presented ordinary

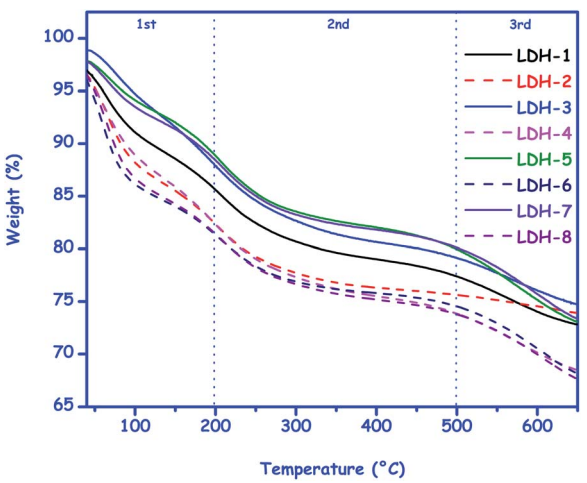


Fig. 7 TGA results highlighting the two sets of samples.

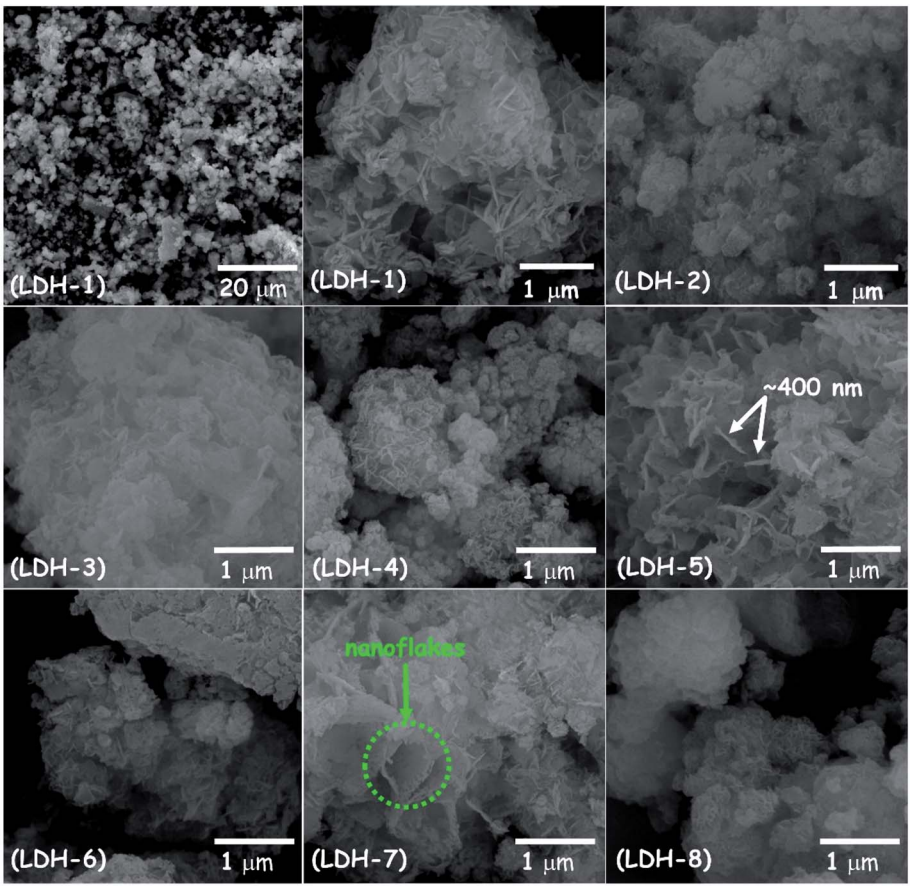


Fig. 8 SEM results for LDHs emphasizing the formation of nanoflakes.

aggregates apparently formed by small crystallites. The other LDH images showed a similar profile under the same magnification and, for this reason, were not shown. However, at 50 000 times of magnification, LDHs displayed sheet-like crystallites[48] arranged as randomly stacked nanoflake type structures. Once again, it was possible to notice that the synthesis conditions had an important influence on the size of the crystallites. Those LDHs labeled with odd numbering, which were submitted to heating during their syntheses, showed higher crystallites.

On the other hand, the LDHs labeled with even numbering, those that were prepared under room temperature, presented smaller crystallites. A closer analysis reveals that, although LDH-3 and LDH-7 were submitted to the same experimental conditions, except for the amount of $NaAlO_2$ (Table 1), the size of the LDH-7 crystallites was larger than that for LDH-3. This result suggests that the mass balance of WPA and $NaAlO_2$ is essential to find the best stoichiometric relationship for the formation of the largest crystallites. In addition, monitoring of $Fe^{2+}/Fe^{3+}$ molar ratio and its oxidation process is mandatory in order to prevent unnecessary excesses of $NaAlO_2$.

## 4 Conclusion

A greener co-precipitation method was studied and presented as an alternative to the low-tech precipitation with lime commonly used for the WPA treatment. A zinc–iron–aluminum-based LDH containing chloride was successfully synthesized from waste pickling acid and sodium aluminate produced from secondary industrial sources. The sustainability profile of the research was supported by the use of a single high quality chemical, the sodium hydroxide, which was necessary to adjust the desirable pH for the syntheses. The supernatant of the synthesis presented low metal content and could be recycled in the system itself as a blend for a fresh sodium hydroxide solution. The eight LDHs were characterized and presented the main features normally known for hydrotalcite-like compounds, such as a defined interlayer space, sheet-like structures and slit-shaped pores. The size of the crystallites was strongly influenced by the experimental conditions used in the syntheses, considering that the temperature and WPA/$NaAlO_2$ molar ratio played the most relevant role in order to control the LDH formation. According to the general results, the method presented in this work allows us to infer that the presence of zinc and iron makes these LDHs an excellent candidate for alternative sorbents for the removal of $H_2S$.

## Conflicts of interest

There are no conflicts to declare.

## Acknowledgements

The authors acknowledge the financial support obtained from CAPES (Coordenação de Aperfeiçoamento de Pessoal de Nível Superior) and CNPq (Conselho Nacional de Desenvolvimento Científico e Tecnológico). They are also thankful for the technical support of the LAMAP and LabMult – the Multi-User Laboratories of UTFPR (Universidade Tecnológica Federal do Paraná).

## References

1 The United Nations, https://www.un.org/sustainabledevelopment/development-agenda/ (accessed January 2021).
2 R. A. Sheldon, *Green Chem.*, 2016, **18**, 3180–3183.
3 A. Chalmers, *The Scientist's Atom and the Philosopher's Stone,* Springer, New York, 2009.
4 A. Nayak and B. Bhushan, *J. Environ. Manage.*, 2019, **233**, 352–370.
5 N. Ferronato and V. Torretta, *Int. J. Environ. Res. Public Health*, 2019, **16**, 1–28.
6 J. E. Rutkowski and E. W. Rutkowski, *Waste Manage. Res.*, 2015, **33**, 1084–1093.
7 S. Sanghvi, N. Pereira, A. Halajko and G. G. Amatucci, *RSC Adv.*, 2014, **4**, 57098–57110.
8 D. Dwivedi, K. Lepková and T. Becker, *RSC Adv.*, 2017, **7**, 4580–4610.
9 World Steel Association, https://www.worldsteel.org/steel-by-topic/statistics/ (accessed January 2021).
10 C. Magazzino, M. Mele, N. Schneider and S. A. Sarkodie, *Sci. Total Environ.*, 2021, **755**, 1–15.
11 E. Jarosz-Kremińska, E. Helios-Rybicka and M. Gawlicki, *Int. J. Environ. Sci. Technol.*, 2014, **12**, 2901–2908.
12 M. Regel-Rosocka, *J. Hazard. Mater.*, 2010, **177**, 57–69.
13 L. Pietrelli, S. Ferro and M. Vocciante, *Chem. Eng. J.*, 2018, **341**, 539–546.
14 L. Wang, Q. Li, Y. Li, X. Sun, J. Li, J. Shen, W. Han and L. Wang, *J. Waste Manage.*, 2018, **71**, 411–419.
15 A. Arguillarena, M. Margallo, A. Arruti-Fernández, J. Pinedo, P. Gómez and A. Urtiaga, *Membranes*, 2020, **10**, 1–14.
16 M. T. A. Reis and M. R. C. Ismael, *Phy. Sci. Rev.*, 2018, **3**, 1–24.
17 L. Gao, J. Chen, C. Tang, Z. Ke, J. Wang, Y. Shimizu and A. Zhu, *Environ. Sci.: Processes Impacts*, 2015, **17**, 1769–1782.
18 A. Devi, A. Singhal, R. Gupta and P. Panzade, *Clean Technol. Environ. Policy*, 2014, **16**, 1515–1527.
19 N. Y. Ghare, K. S. Wani and V. S. Patil, *J. Environ. Sci. Eng.*, 2013, **55**, 253–266.
20 L. Mohapatra and K. Parida, *J. Mater. Chem. A*, 2016, **4**, 10744–10766.
21 S. Miyata, *Clays Clay Miner.*, 1983, **31**, 305–311.
22 M. Laipan, J. Yu, R. Zhu, J. Zhu, A. T. Smith, H. He, D. O'Hare and L. Sun, *Mater. Horiz.*, 2020, **7**, 715–745.
23 S. Samuei, F. Arjamandi Rad and Z. Rezvani, *Appl. Clay Sci.*, 2020, **184**, 1–9.
24 W. Huo, T. Cao, X. Liu, W. Xu, B. Dong, Y. Zhang and F. Dong, *Green Energy Environ.*, 2019, **4**, 270–277.
25 J. Li, L. Yan, Y. Yang, X. Zhang, R. Zhu and H. Yu, *New J. Chem.*, 2019, **43**, 15915–15923.
26 R. Sasai, H. Sato, M. Sugata, T. Fujimura, S. Ishihara, K. Deguchi, S. Ohki, M. Tansho, T. Shimizu, N. Oita, M. Numoto, Y. Fujii, S. Kawaguchi, Y. Matsuoka, K. Hagura, T. Abe and C. Moriyoshi, *Inorg. Chem.*, 2019, **58**, 10928–10935.
27 L. E. G. Rodriguez, A. Bail, R. O. Castillo and G. G. C. Arízaga, *Curr. Pharm. Des.*, 2020, **26**, 1–14.
28 N. B. Allou, P. Saikia, A. Borah and R. L. Goswamee, *Colloid Polym. Sci.*, 2017, **295**, 725–747.
29 M.-S. Kim, T.-H. Kim, Y. S. Seo, J.-M. Oh and J. K. Park, *Dalton Trans.*, 2017, **46**, 7656–7659.
30 C. Ruby, M. Usman, S. Naille, K. Hanna, C. Carteret, M. Mullet, M. François and M. Abdelmoula, *Appl. Clay Sci.*, 2010, **48**, 195–202.
31 M. P. Figueiredo, V. R. R. Cunha, F. Leroux, C. Taviot-Gueho, M. N. Nakamae, Y. R. Kang, R. B. Souza, A. M. C. R. P. F. Martins, I. H. J. Koh and V. R. L. Constantino, *ACS Omega*, 2018, **3**, 18263–18274.
32 A. Golban, L. Lupa, L. Cocheci and R. Pode, *Crystal*, 2019, **9**, 1–15.
33 M. K. R. Reddy, Z. P. Xu, G. Q. Lu and J. C. D. da Costa, *Ind. Eng. Chem. Res.*, 2006, **45**, 7504–7509.
34 C. Megías-Sayago, R. Bingre, L. Huang, G. Lutzweiller, Q. Wang and B. Louis, *Front. Chem.*, 2019, **7**, 1–10.
35 S. Lee, M. Govindan and D. Kim, *Chem. Eng. J.*, 2021, **416**, 127918.
36 T. N. D. Cunha, D. G. Trindade, M. M. Canesin, L. Effting, A. A. de Moura, M. P. Moisés, I. L. Costa Junior and A. Bail, *Waste Biomass Valorization*, 2021, **12**, 1517–1528.
37 S. Brunauer, P. H. Emmet and E. Teller, *J. Am. Chem. Soc.*, 1938, **60**, 309–319.
38 E. P. Barrett, L. G. Joyner and P. P. Halenda, *J. Am. Chem. Soc.*, 1951, **73**, 373–380.
39 R. Baird and L. Bridgewater, *Standard Methods for the Examination of Water and Wastewater*, American Public Health Association, Washington, D.C., 2017.
40 J. J. Gil, O. Aguilar-Matínez, Y. Piña-Pérez, R. Pérez-Hernández, C. E. Santolalla-Vargas, R. Gómez and F. Tzompantzi, *Renewable Energy*, 2020, **145**, 124–132.
41 D. Li, L. Ouyang, L. Yao, L. Zhu, X. Jiang and H. Tang, *ChemistrySelect*, 2018, **3**, 428–435.
42 Y. Zhang and J. R. G. Evans, *Colloids Surf., A*, 2012, **408**, 71–78.
43 T. Kameda, T. Yoshioka, F. Yabuuchi, M. Uchida and A. Okuwaki, *Bull. Mater. Sci.*, 2008, **31**, 625–629.
44 F. Z. Mahjoubi, A. Khalidi, M. Abdennouri and N. Barka, *J. Taibah Univ. Sci.*, 2017, **11**, 90–100.
45 C. Chen, K. Ruengkajorn, J.-C. Buffet and D. O'Hare, *RSC Adv.*, 2018, **8**, 34650–34655.
46 G. Lian, Z. Fen, L. Jun-Cai, Z. Rong-Chang, Li Shuo-Qi, S. Liang and Z. Jian-Min, *Front. Mater. Sci.*, 2018, **12**, 198–2016.
47 C.-C. Huang, C.-H. Chen and S.-M. Chu, *J. Hazard. Mater.*, 2006, **136**, 866–873.
48 J. L. Gunjakar, I. Y. Kim, J. M. Lee, N.-S. Lee and S.-J. Hwang, *Energy Environ. Sci.*, 2013, **6**, 1008–1017.